Laser & Photonics Reviews

LASER & PHOTONICS REVIEWS

www.lpr-journal.org

RESEARCH ARTICLE

Efficient and Stable Flexible PeLEDs Enabled by Polymer Interfacial Permeation Engineering

Hailiang Huang[1] | Zhibin Wang[1] | Song Zheng[1] | Ximing Wu[1] | Tao Pang[2] | Lingwei Zeng[3] | Yongping Zheng[1] | Ruidan Zhang[1] | Feng Huang[1] | Daqin Chen[1,4]

[1]College of Physics and Energy, Fujian Provincial Key Laboratory of Quantum Manipulation and New Energy Materials, Fujian Normal University, Fuzhou, P. R. China | [2]Huzhou Key Laboratory of Materials for Energy Conversion and Storage, College of Science, Huzhou University, Huzhou, Zhejiang, P. R. China | [3]School of Chemistry and Chemical Engineering, Key Laboratory of Theoretical Organic Chemistry and Functional Molecule of Ministry of Education, Hunan University of Science and Technology, Xiangtan, Hunan, P. R. China | [4]Fujian Provincial Engineering Technology Research Center of Solar Energy Conversion and Energy Storage, Fujian Normal University, Fuzhou, Fujian, P. R. China

Correspondence: Zhibin Wang (zhibinwang@fjnu.edu.cn) | Yongping Zheng (zyp@fjnu.edu.cn) | Daqin Chen (dqchen@fjnu.edu.cn)

Received: 19 September 2025 | **Revised:** 1 April 2026 | **Accepted:** 8 April 2026

Keywords: flexible perovskite light-emitting diodes | operational stability | polymer | power conversion efficiency | sub-bandgap emission

ABSTRACT

Flexible perovskite light-emitting diodes (f-PeLEDs) hold great promise for next-generation optoelectronics, but their efficiency and operational half-lifetime (T_{50}) remain limited by poor film quality on deformable substrates. Herein, we develop a polymer interfacial permeation strategy by incorporating poly(2-ethyl-2-oxazoline) (PEOXA) into the hole transport layer (HTL). Through an antisolvent-free one-step spin-coating process, PEOXA spontaneously partitions between the HTL and perovskite emitting layer, forming a 3D interpenetrating network that simultaneously passivates defects and enhances mechanical flexibility. The carbonyl groups in the polymer chains act as Lewis bases, simultaneously improving luminescence efficiency and enhancing crystallinity. Meanwhile, the polymer incorporation reduces the Young's modulus, significantly boosting device flexibility. These synergistic effects enable green f-PeLEDs to achieve a record-high peak external quantum efficiency of 23.4% along with a power conversion efficiency of 26.7%, and demonstrate exceptional operational stability, with a measured T_{95} lifetime of 3.2 h at an initial luminance of 1000 cd/m^2. This work thereby establishes a versatile and robust strategy for the development of high-performance, flexible perovskite optoelectronics.

1 | Introduction

Metal halide perovskites have emerged as highly promising candidates for next-generation optoelectronic applications, particularly in flexible displays and solid-state lighting [1–3]. Recent research has demonstrated substantial improvements in the performance of perovskite light-emitting diodes (PeLEDs) fabricated on rigid substrates. Through systematic optimization approaches including morphology engineering [4, 5], dimensionality control [6, 7], and defect passivation [8–10], the external quantum efficiencies (EQE) of PeLEDs have approached their theoretical limits [11–13]. However, flexible perovskite light-emitting diodes (f-PeLEDs) typically exhibit lower device efficiency and operational half-lifetime (T_{50}) compared to their rigid counterparts [14–22]. This performance gap primarily stems from the crystalline quality of perovskite films on flexible substrates struggling to match that on rigid substrates. Moreover, f-PeLEDs currently exhibit significantly higher turn-on voltages (V_T) than their corresponding bandgap voltages, which inevitably compromises power conversion efficiency (PCE) and operational stability. For example, state-of-the-art green f-PeLEDs (EQE_{max} = 22.1%) currently achieve a maximum PCE of 8.6% and a V_T of 3.5 V, yet

exhibit a limited T_{50} of 52 min at initial luminance of 1000 cd/m^2 [23]. Therefore, developing f-PeLEDs that combine high PCE, long T_{50}, and excellent mechanical robustness is crucial for meeting and advancing the developmental needs of future flexible display technologies.

Improving the optoelectronic performance and mechanical stability of f-PeLEDs remains a critical challenge. Recent efforts have focused on optimizing flexible electrodes/substrate [24–26], additive engineering [27], morphology control [28], and light extraction engineering [29]. For instance, Qin et al. developed a poly(methyl methacrylate) (PMMA)-modified label paper substrate. The PMMA coating not only physically smoothed the rough surface of the paper but also enhanced wettability through its porous structure and hydrophilic surface properties [30]. Wei et al. successfully fabricated dendritic $CsSnI_3$ structure by precisely modulating precursor concentration, thereby significantly enhancing the bending durability of flexible devices [28]. While existing approaches enhance f-PeLEDs performance, they often overlook critical interfacial challenges in multilayer architectures, particularly the mechanical mismatch between perovskite and charge transport layers. Conventional organic hole transport layers (HTLs), for instance, exhibit significantly different Young's moduli compared to inorganic emissive layers. This mechanical disparity becomes particularly problematic under external stress, where strain incompatibility leads to interfacial delamination, film cracking, and defect proliferation, ultimately accelerating device degradation [31]. Thus, an integrated, facile strategy concurrently enhancing interfacial integrity and suppressing defects is urgently needed for high-performance and stable f-PeLEDs.

Polymers, with their extended molecular chains and versatile functional groups, offer a dual advantage in modulating perovskite crystallization while simultaneously enhancing the mechanical stability of flexible devices. Studies have demonstrated that polymers with specific functional groups (e.g., isocyanate (—N═C═O), disulfide (—S—S—)) strengthen perovskite interactions, thereby improving device mechanical properties [32]. These modifiers are typically introduced either by direct mixing into the perovskite precursor solution [33, 34] or via antisolvent-assisted crystallization [23]. For instance, incorporating diphenylmethane diisocyanate polyurethane into precursor solutions enable heat-activated self-healing of bending cracks due to the intra/intermolecular hydrogen bonds [34]. Choy et al. demonstrated that introducing polyvinyl acetate through antisolvent engineering yielded green f-PeLEDs achieving a record 22.1% EQE [23]. Nevertheless, this approach faces limitation as most antisolvents are both toxic and poorly suited for scalable production. More fundamentally, these strategies remain inadequate for addressing the performance bottlenecks, as their singular focus on monolayer optimization fails to tackle the intricate interfacial challenges inherent to multilayer heterostructures.

In this study, we propose a polymer interfacial permeation strategy by incorporating poly(2-ethyl-2-oxazoline) (PEOXA), into the HTL. PEOXA simultaneously modulates perovskite crystallization and passivates grain boundary defects. During spin-coating of the emissive layer, partial PEOXA dissolves into dimethyl sulfoxide (DMSO), enabling its permeation into the perovskite film. It then permeates into the grain boundary regions of the perovskite film, forming a 3D interpenetrating network structure at the HTL/perovskite interface and within the perovskite bulk. The 3D interpenetrating network simultaneously improved mechanical compliance and device performance, yielding green f-PeLEDs with a PCE of 26.7%. The resulting devices also demonstrated exceptional operational stability, exhibiting a measured T_{95} lifetime of 3.2 h at an initial luminance of 1000 cd/m^2.Consequently, this work establishes a promising and practical pathway for the integration of perovskite materials into next-generation flexible electronics.

2 | Results and Discussion

During spin-coating process, flexible substrates frequently undergo deformation, leading to inhomogeneous crystallization in subsequently deposited perovskite films. This crystallization non-uniformity represents a key factor contributing to the performance disparity between flexible and rigid devices. To address these challenges, we evaluated three common substrate-fixation strategies in f-PeLEDs fabrication (Figure 1a). Three fixation approaches were implemented: direct mounting of the PEN substrate on a porous vacuum chuck (Strategy A); adhesive attachment to a size-matched glass slide using polyimide tape prior to spin-coating (Strategy B); and polydimethylsiloxane (PDMS)-mediated bonding to a rigid glass slide via screen-printing (Strategy C). Notably, the f-PeLEDs exhibited substantial EQE variations depending on the fabrication strategy (Figure S1 and Table S1), with values of 4.2%, 11.9%, and 19.9% achieved for Strategies A, B, and C, respectively. The normalized EL spectra exhibit a narrowing of full width at half maximum (FWHM) from 22.2 to 17.1 nm, suggesting enhanced crystalline uniformity achieved via substrate fixation optimization. These spectral improvements, together with the EQE enhancement, demonstrate the critical role of PEN substrate flatness and rigidity in spin-coating processes. Strategies A and B produced substantial PEN substrate undulations exceeding the total functional layer thickness, leading to non-uniform perovskite morphology. Further observations showed that even with Strategy C, bubbles in the PDMS adhesion layer are detrimental to device performance. In the region with bubbles, the EQE dropped from an initial 19.9% to 9.4% (Figure S2). This phenomenon supports our hypothesis that substrate flatness critically influences film quality and ultimate device performance.

Furthermore, interactions at the interface between the buried layer and the perovskite precursor solution critically influence the microscale morphology of the resulting emissive film. Building on these insights, we developed a polymer-mediated interface by incorporating PEOXA into the HTL. This approach harnesses the dual functionality of PEOXA: its hydrogen-bonding groups strengthen interfacial adhesion with the perovskite layer, while its Lewis basic character passivates surface defects. This synergistic effect arises from solvent-assisted interfacial reorganization during perovskite deposition (Figure 1b). During spin-coating process of the perovskite precursor solution (in DMSO), PEOXA partially dissolves and migrates from the HTL into the forming perovskite film. This dynamic process creates a 3D interpenetrating network that permeates both interfacial regions and grain boundaries. The resulting architecture provides two key benefits: (1) chemical passivation through Lewis base coordination, where PEOXA's carbonyl groups bind to undercoordinated Pb^{2+} sites,

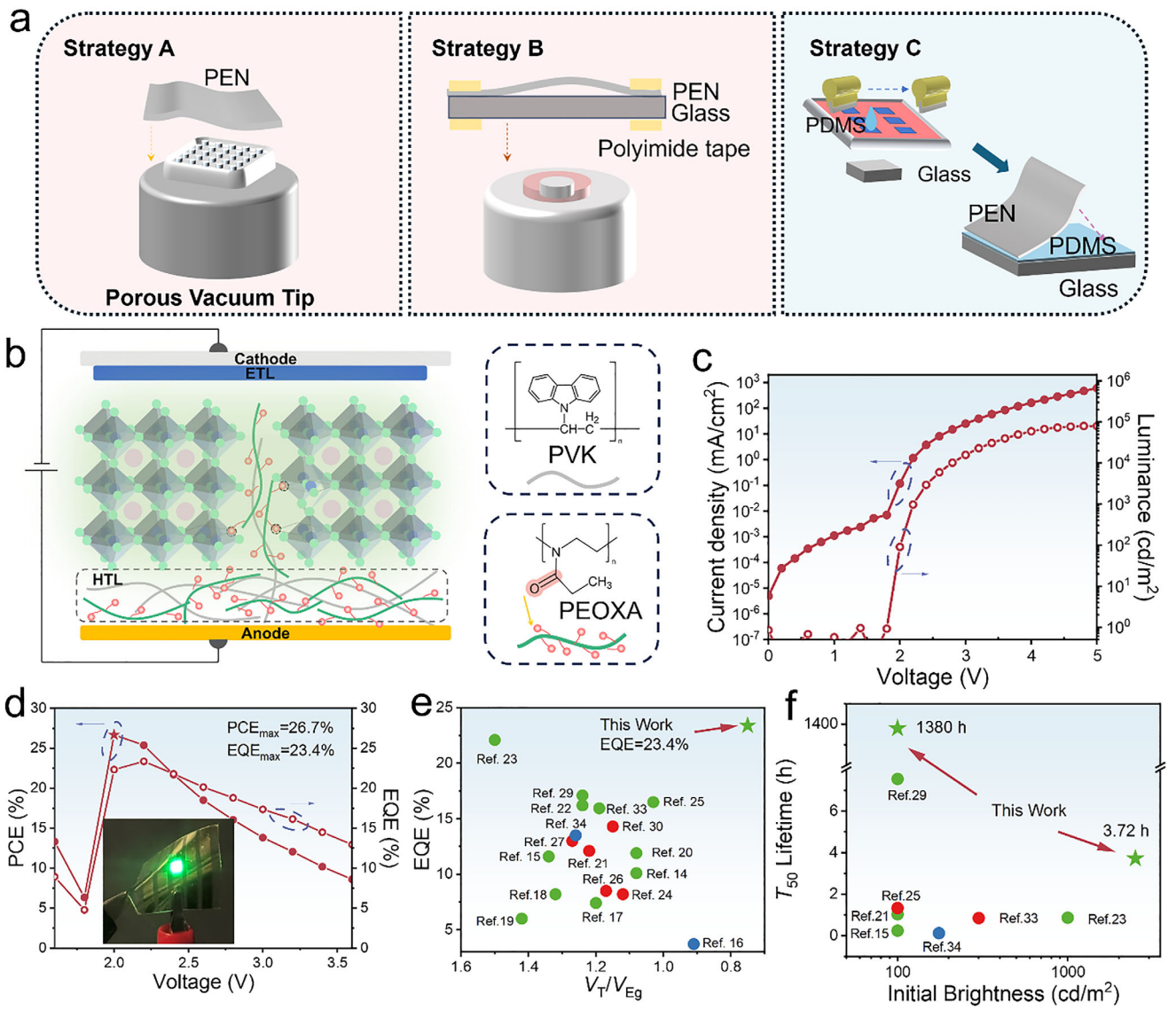

FIGURE 1 | (a) Schematic illustration of various substrate fixing strategies. (b) Schematic illustration of the working mechanism of the polymer interfacial permeation strategy. (c) Current density–voltage–luminance (*J*--*V*--*L*) characteristic curves and (d) power conversion efficiency (PCE) and external quantum efficiency (EQE) versus *V* curves of the optimized f-PeLEDs. (e) Comparison of the ratio of turn-on voltage (V_T) to bandgap voltage (V_{Eg}) for previously reported f-PeLEDs. (f) Comparison of the operational half-lifetime (T_{50}) of our optimized f-PeLEDs devices with other works.

suppressing defect-mediated nonradiative recombination; and (2) mechanical reinforcement via modulus reduction, as the PEOXA network lowers the Young's modulus of emissive layer, enhancing both intrinsic flexibility and device bending durability.

To validate this polymer interfacial permeation modification strategy, f-PeLEDs were fabricated using the optimized flexible substrate fixing strategy (Strategy C), and their optoelectronic properties were characterized. The device architecture was PEN substrate/poly[bis(4-phenyl)(2,4,6-trimethylphenyl)amine] (PTAA)/poly(9-vinylcarbazole) (PVK) /perovskite/2,4,6-tris[3-(diphenylphosphinyl)phenyl]-1,3,5-triazine (PO-T2T)/LiF/Al. To optimize device performance, we systematically varied the PEOXA concentration from 0 to 4 mg/mL. The performance metrics exhibited a clear optimum, with the highest efficiency achieved at 2 mg/mL, which was consequently selected as the optimal concentration (Figure S3 and Table S2). Device performance was first evaluated by comparing the current density–voltage–luminance (*J*–*V*–*L*) characteristics of the devices (Figure 1c; Figure S4). The optimized PEOXA device achieved a L_{max} of 79925 cd/m^2, a nearly 2.5-fold enhancement over the control device (32295 cd/m^2).

As illustrated in Figure 1d, the PEOXA-modified PeLEDs achieve a maximum EQE of 23.4%, coupled with a low V_T of 1.8 V, which is 75% of the bandgap voltage (~2.4 V). While some f-PeLEDs architectures in the literature report high EQE, their V_T values often substantially exceed the bandgap voltage (V_{Eg}) [22, 23, 29]. This high operating voltage severely limits the PCE, which typically remains below 15% and is considerably lower than the corresponding EQE (Table S3). Excessively high V_T leads to significant energy loss through Joule heating, raising the device temperature and consequently degrading operational stability and lifetime. Therefore, minimizing V_T is essential for developing

stable devices. In this study, our strategy uniquely delivers a combination of high EQE and low operating voltage, resulting in an exceptional PCE of 26.7%. This result surpasses the PCE of 23.7% obtained from the control device (Figure S5). The inset depicts an operational f-PeLEDs emitting bright green light at 519 nm, with a narrow spectral bandwidth of 17.0 nm (Figure S6) [35]. To the best of our knowledge, these values represent the highest reported EQE and PCE for green f-PeLEDs to date (Figure 1e). To rigorously confirm the performance enhancement provided by PEOXA and exclude fabrication-related variations, we conducted a statistical analysis of 30 individual devices (Figure S7). Control devices (w/o PEOXA) showed significant performance fluctuations, with an average EQE of 14.32% and a large standard deviation of 2.49%. In contrast, the PEOXA-modified PeLEDs exhibited markedly improved consistency, achieving a higher average EQE of 21.77% with a narrow efficiency distribution (standard deviation = 0.98%).

As mentioned above, operating voltages below the V_{Eg} reduce Joule heating and suppress electric field-driven ion migration within the perovskite emitter, which significantly enhances operational longevity [36, 37]. The champion device demonstrated a T_{50} lifetime of 3.72 h at an initial brightness of 2500 cd/m^2. Based on the accelerated lifetime equation ($L_0^n \times T_{50}$ = constant, where n is an acceleration factor, calculated to be 1.73 in this case), the projected T_{50} lifetime reaches 1380 h at 100 cd/m^2. The optimized f-PeLEDs exhibits exceptional operational stability, exceeding previously reported benchmarks (Figure 1f). To validate the general applicability of our approach, we fabricated rigid devices with an identical architecture. As anticipated, these devices exhibited comparable performance improvements (Figure S8). These results demonstrate that the polymer interfacial penetration strategy is a robust and broadly applicable method for realizing high-performance f-PeLEDs.

To verify the effectiveness of our polymer interfacial permeation strategy and understand its underlying mechanism, we first examined the distribution of PEOXA within the perovskite films using X-ray photoelectron spectroscopy (XPS) depth profiling. By tracking the characteristic oxygen (O) signal, we observed a slight increase in oxygen content near the surface (within ~15 nm depth), which may originate from surface-adsorbed oxygen or minor surface oxidation [23]. Beyond this surface region, the oxygen concentration increases significantly with etching depth (Figure 2a). This distinct gradient indicates that PEOXA, carried by the solvent from the HTL, permeates into the perovskite film during spin-coating of the emissive layer and accumulates near the HTL interface. These results suggest that PEOXA forms a polymer-enriched interfacial zone during film deposition, which likely modifies local nucleation conditions and enhances perovskite crystallization.

To further understand PEOXA behavior during spin-coating, we analyzed the surface morphology of PEOXA-containing HTL layers using atomic force microscopy (AFM) before and after DMSO washing (Figure 2b). The root-mean-square (RMS) roughness of the PVK:PEOXA surface increased substantially from 0.65 to 1.96 nm following solvent treatment, revealing significant microstructural changes. Control experiments with pure PVK and PEOXA films showed minimal roughness changes under identical conditions (Figure S9). These pronounced morphological alterations suggest DMSO-induced dissolution and subsequent redistribution of PEOXA within the HTL surface.

XPS depth profiling also monitored binding energy changes with depth for various elements (Figure 2c,d). With increasing etching depth, perovskite Pb $4f_{5/2}$ and $4f_{7/2}$ binding energies rose from 142.9 and 138.1 eV (surface) to 143.6 and 138.7 eV (~45 nm depth), respectively. Concurrently, O 1s binding energy trended oppositely, decreasing from 532.4 eV (surface) to 531.7 eV. These opposing depth-dependent binding energy trends evidence interaction between PEOXA and perovskite components [38]. Given the PEOXA molecular structure, we speculate that its chain carbonyl groups (—C═O) act as Lewis base sites. These sites then form effective chemical interactions with Lewis acidic uncoordinated Pb^{2+} ions in the perovskite, thereby passivating these defects. Furthermore, additional peaks observed at 141.6 and 136.8 eV correspond to the 0D Cs_4PbBr_6 phase, consistent with prior reports [39]. The formation of the 0D phase stems from an excess of CsBr and FABr in the perovskite precursor. Specifically, FABr promotes the conversion of excess CsBr into the 0D phase on the surface of the 3D perovskite phase and aligns with our prior findings [36].

To verify the interaction between PEOXA and perovskite precursors, we performed Fourier transform infrared (FTIR) spectroscopy on both pure PEOXA and PEOXA/$PbBr_2$ mixtures (Figure 2e). The characteristic carbonyl (—C═O) stretching vibration of pure PEOXA appears at 1636 cm^{-1}, while in PEOXA/$PbBr_2$ mixtures the corresponding peak shifts significantly to 1623 cm^{-1}. The redshift demonstrates strong coordination between Pb^{2+} ions and the lone pair electrons located on the carbonyl oxygen, corroborating our XPS observations of interfacial interactions [40]. To gain deeper insight into solution-phase interactions, we conducted ^{1}H nuclear magnetic resonance (NMR) spectroscopy on PEOXA-perovskite precursor mixtures in deuterated solvents (Figure 2f). The NMR spectra revealed chemical shifts in proton signals from PEOXA as well as from the organic cations PEA^+ and FA^+. These shifts indicate that the carbonyl groups of PEOXA interact not only with Pb^{2+} ions but also form hydrogen bonds with the amino groups (-NH_3^+ or -NH_2^+) of the organic cations. Such interactions modify the local chemical environment, accounting for the observed spectral changes [41, 42]. These solution-phase findings complement our FTIR results, collectively demonstrating that PEOXA effectively passivate defects through multiple coordination mechanisms.

The optical properties of perovskite films critically influence f-PeLEDs performance. Photoluminescence (PL) measurements reveal that PEOXA-modified films exhibit sharper emission peaks (Figure S10) with a 20% increase in PL intensity and a marginal narrowing of the FWHM from 18.8 to 18.5 nm compared to control films. While FWHM alone does not directly reflect crystallinity [43], the combined enhancement in PL intensity and spectral narrowing suggests suppressed non-radiative recombination and reduced defect density [44, 45]. These observations provide initial evidence that PEOXA incorporation effectively passivates trap states in the perovskite films. To quantify the effect of PEOXA modification on trap state density, hole-only devices with an architecture of ITO/PTAA/PVK/perovskite/MoO_3/Ag were fabricated (Figure S11). The trap-filled limit voltage (V_{TFL}), determined from space-charge-limited current (SCLC) measurements, serves

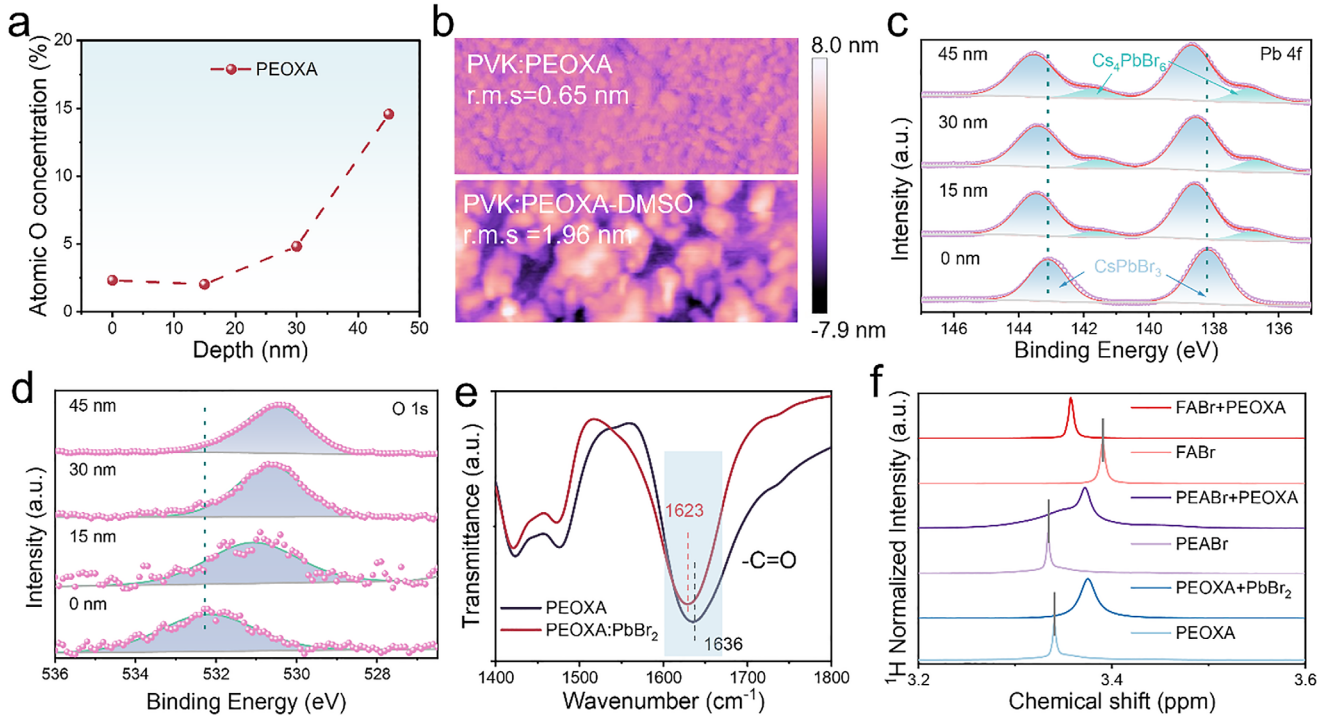

FIGURE 2 | (a) Depth profile of the oxygen content in PEOXA-treated films. (b) AFM images of the HTL before and after DMSO treatment. Depth profiles of elemental binding energy for (c) lead, and (d) oxygen. (e) FTIR spectra of pure PEOXA and the PEOXA/$PbBr_2$ mixture. (f) ^1H NMR spectra of PEOXA and a mixture of PEOXA with perovskite precursor components in deuterated solution.

as a sensitive indicator of trap state density. PEOXA incorporation reduced the V_{TFL} significantly from 0.97 to 0.80 V, suggesting a substantial decrease in trap states. The corresponding defect density (n_t) of the film is obtained by the following equation [46]:

$$n_t = \frac{2V_{TFL}\varepsilon\varepsilon_0}{eL^2}$$

where ε is the relative permittivity, ε_0 represents vacuum permittivity, L is the thickness of the perovskite layer, and e is the elementary charge ($e = 1.6 \times 10^{-19}$ C). The calculated defect density decreases from1.44×10^{17} to 1.19×10^{17} cm^{-3}, demonstrating that PEOXA modification effectively reduces trap states in the perovskite film.

To gain a deeper understanding of the effect of PEOXA modification on the carrier dynamics of perovskite films, we performed femtosecond transient absorption (TA) spectroscopy tests. Figure 3a,b respectively show the pseudo-color TA maps of perovskite thin film with various modification strategies under 400 nm excitation. To ensure the study was conducted under low carrier density conditions and to exclude the influence of many-body interactions among carriers and Auger recombination processes, we used a low pump energy of 1.07 μJ cm^{-2} [47]. In the spectra of both samples, a typical ground-state bleach (GSB) signal located at approximately 505 nm can be observed [36]. Subsequently, we performed a global fit on the TA decay kinetic curves using a tri-exponential decay model convoluted with the instrument response function (Figure 3c), and the parameters of the fitted decay components are summarized in Table S4. According to the fitting results, we deconvoluted the carrier decay process in the perovskite films into three stages: the fastest decay stage (I) is mainly attributed to the rapid trapping of carriers by shallow traps; the intermediate decay component (II) is related to defect-assisted non-radiative recombination processes; and the slow decay process (III) represents the radiative recombination of electron-hole pairs [48, 49]. By comparing the fitting parameters, we found that in the PEOXA-modified film, the increased amplitude proportion (A_3) coupled with a shorter radiative recombination lifetime (τ_3) indicates enhanced radiative recombination rates. Meanwhile, the reduced contribution from defect-trapping process (τ_1) suggests suppressed non-radiative recombination pathways, these effects lead to significantly improved photoluminescence efficiency in the PEOXA-modified films.

We further performed time-resolved photoluminescence (TRPL) spectroscopy measurements (Figure 3d). TRPL decay curves were fitted using a bi-exponential decay model to calculate average carrier lifetimes (τ_{ave}). Detailed fitting parameters and τ_{ave} are summarized in Table S5. Fitting results show PEOXA-modified perovskite films exhibit a τ_{ave} of 63.9 ns, approximately 20% longer than that of control films (53.8 ns). To quantify luminescence efficiency, we further measured photoluminescence quantum yield (PLQY) (Figure 3e). The PEOXA-modified films achieved a PLQY of 84.52%, representing a significant improvement over the control films (63.22%). The radiative (k_r) and non-radiative (k_{nr}) recombination rates in perovskite films can be calculated using the following equations [50, 51]:

$$PLQY = \frac{k_r}{k_r + k_{nr}}$$

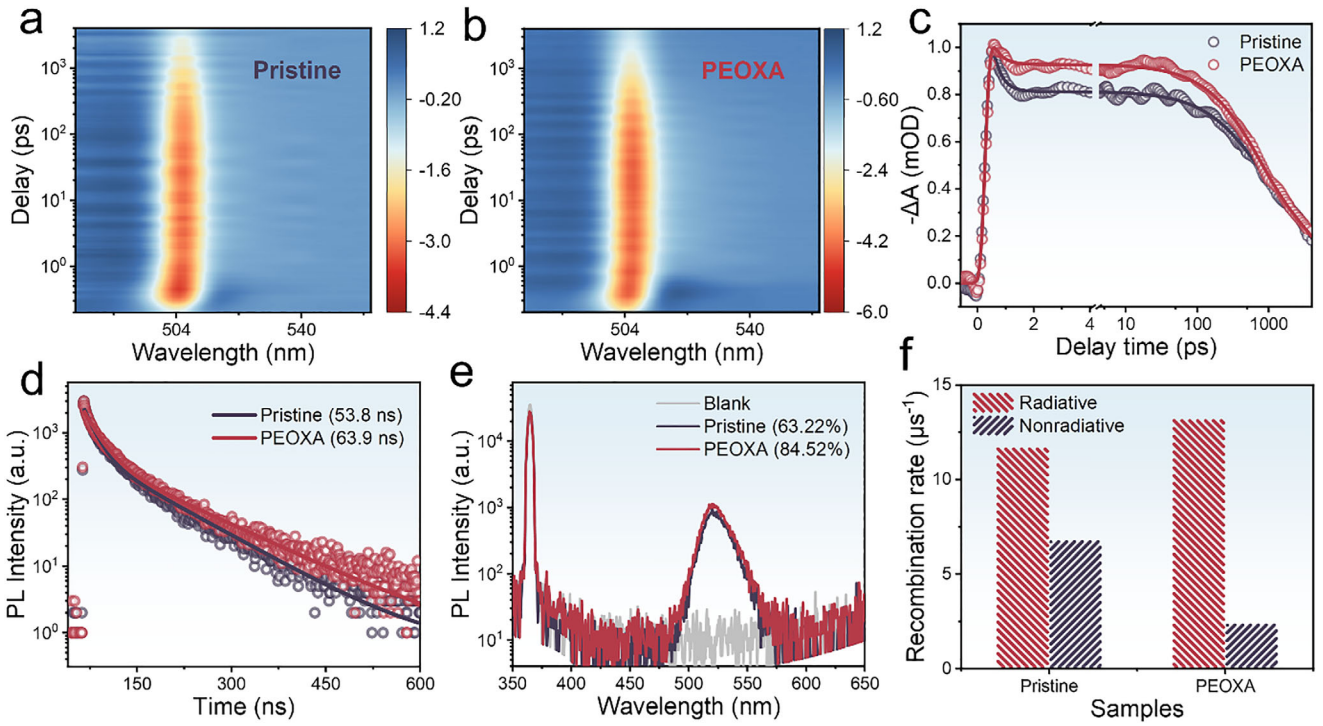

FIGURE 3 | Pseudocolor maps of fs-transient absorption spectra of (a) the control film and (b) the PEOXA-modified film. (c) Carrier decay kinetic curves at the 505 nm photobleaching peak, (d) TRPL spectra, (e) PLQY, and (f) radiative and non-radiative recombination rates of the control and PEOXA-modified films.

$$\tau_{ave} = \frac{1}{k_r + k_{nr}}$$

Data analysis indicates that PEOXA incorporation moderately increased the radiative recombination rate (k_r) from 11.7 to 13.2 μs^{-1}, while significantly decreasing the non-radiative recombination rate (k_{nr}) from 6.8 to 2.4 μs^{-1} (Figure 3f). The results suggest that the high PLQY achieved through PEOXA modification is primarily due to the suppression of non-radiative recombination via defect passivation [52].

To highlight the advantages of PEOXA, we compared it with poly(ethylene oxide) (PEO), a structurally similar and widely referenced polymer. We first used density functional theory (DFT) calculations to compare the coordination ability of the carbonyl group in PEOXA with the ether (C—O—C) linkages in PEO. The results show that PEOXA has a significantly more favorable adsorption energy (−0.124 eV/atom) on undercoordinated Pb^{2+} sites than PEO (−0.069 eV/atom). Molecular electrostatic potential (ESP) mapping further identifies electron-rich regions in PEOXA that facilitate strong anchoring to Pb^{2+} centers (Figure S12). Experimental measurements of PLQY and lifetime support these theoretical predictions. Although PEO-modified films show notable improvements over the pristine sample, they underperform relative to PEOXA. The PEO-treated film exhibits a lifetime of 60.8 ns and a PLQY of 78.6% (Figure S13), both lower than those achieved with PEOXA. Consistently, the radiative and non-radiative recombination rates for PEO are less favorable than those for PEOXA (Figure S14 and Table S6), in excellent agreement with our calculations.

To evaluate the influence of PEOXA interfacial modification on perovskite crystal structure, we performed X-ray diffraction (XRD) on the resulting films (Figure S15). The PEOXA-modified film exhibited enhanced diffraction peak intensities compared to the control, indicating improved crystallinity. Both films showed signatures of coexisting 0D and 3D phases. Peaks at 15.2°, 21.4°, and 30.4° correspond to the (100), (110), and (200) planes of the cubic $CsPbBr_3$ phase, respectively, while peaks at 12.6° and 30.9° confirm the presence of the 0D Cs_4PbBr_6 phase, a finding consistent with our earlier XPS observations. The presence of 0D phase effectively passivates defects in the 3D phase, leading to a significant enhancement in the luminescent performance of the film [36]. Ultraviolet-visible (UV-vis) absorption spectroscopy (Figure S16) shows nearly identical spectra for both PEOXA-modified and unmodified perovskite films, with no observable shifts or additional absorption features. These results confirm that PEOXA incorporation preserves the original bandgap, phase composition, and emission characteristics of the perovskite material [45]. Concurrently, we investigated the impact of PEOXA on the energy level alignment of the device (Figure S17). For the pristine PVK HTL, the highest occupied molecular orbital (HOMO) level is −5.60 eV. Incorporating PEOXA shifts the HOMO upward to −5.35 eV. Although this shift could, in principle, increase the hole injection barrier, we observed no significant rise in the turn-on voltage. Instead, PEOXA modification clearly enhances both the EQE and maximum luminance of the device. These gains are attributed primarily to the improved perovskite crystallinity and defect passivation afforded by PEOXA, rather than to changes in interfacial energy-level alignment.

The mechanical stability of flexible perovskite devices critically depends on the Young's modulus of their functional layers. To

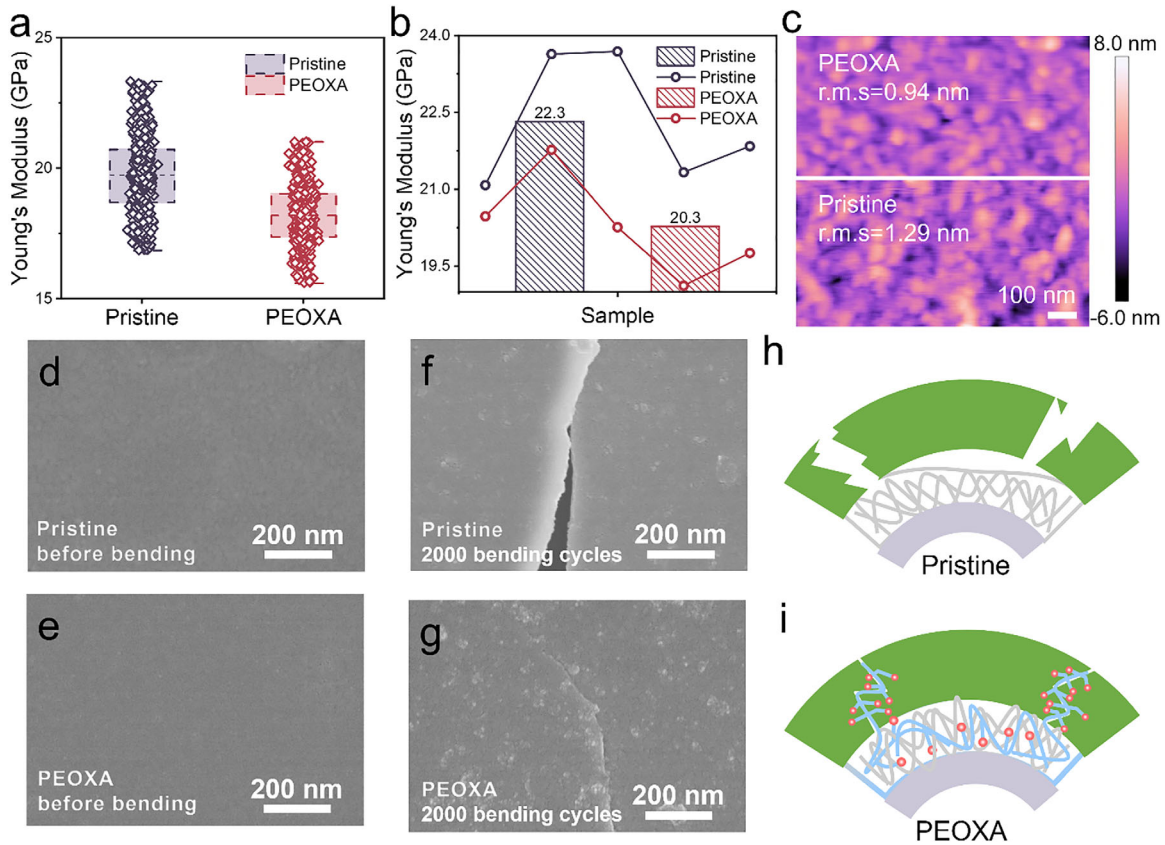

FIGURE 4 | (a) Box plot of Young's modulus, (b) Bar chart of average Young's modulus, (c) AFM image for control and PEOXA-modified films. SEM images before bending of (d) control film, and (e) PEOXA-modified film. SEM images after 2000 bending cycles of (f) control film, and (g) PEOXA-modified film. Schematic of the bending resistance mechanism in (h) the control film, and (i) the PEOXA-modified film.

accurately assess this property, we prepared perovskite films on PTAA/PVK substrates matching actual device architectures and measured their Young's modulus using continuous stiffness measurement (CSM) [31]. PEOXA incorporation reduced the Young's modulus from 22.3 to 20.3 GPa (Figure 4a,b), indicating enhanced elastic deformability. This mechanical softening provides two key benefits: (1) improved bending endurance by facilitating elastic deformation under stress, and (2) reduced mechanical mismatch with the underlying organic HTL, which minimizes interfacial stress concentration and suppresses mechanical failures like film cracking and delamination. These effects collectively enhance the structural integrity of multilayer flexible devices [31]. As shown in Young's modulus distributions and load-displacement curves (Figures S18 and S19), the significant modulus reduction induced by PEOXA is further confirmed.

The quality of perovskite films critically governs charge carrier dynamics and ultimately device performance. AFM characterization reveals that PEOXA modification reduces surface roughness from 1.29 to 0.94 nm (Figure 4c), indicating improved film uniformity. The morphological enhancement corresponds with reduced surface defect density and suppressed non-radiative recombination [53]. To evaluate the effect of PEOXA on mechanical stability, we compared the surface morphology of perovskite films before and after bending for 2000 cycles. As shown in the scanning electron microscopy (SEM) images, the control film appears significant cracks after bending (Figure 4d,e), whereas PEOXA-modified film shows only minor microcracks under identical conditions (Figure 4f,g). This marked contrast demonstrates the effectiveness of PEOXA in improving the mechanical durability of perovskite films. Figure 4h,i illustrates the proposed protection mechanism: PEOXA permeates the perovskite film, forming an interconnected polymer network throughout the bulk and along grain boundaries. When subjected to bending stress, this network effectively dissipates localized mechanical stresses, thereby enhancing the film's fracture resistance. The stress redistribution prevents crack initiation and propagation, significantly improving mechanical stability.

Our strategy imparted perovskite films with excellent optoelectronic and mechanical properties. We used these films as emissive layers in f-PeLEDs to explore their potential for flexible optoelectronic applications. To validate the scalability of our approach, we fabricated large-area f-PeLEDs with a 4 cm^2 active emissive area (Figure 5a). Mechanical bending tests revealed superior performance of PEOXA-modified devices compared to controls (Figure 5b). At a 5 mm bending radius, modified devices maintained 80% of their initial efficiency after 4500 cycles, while control devices degraded to 20% of their initial performance after only 1000 cycles (Figure 5c). This substantial improvement highlights the effectiveness of our strategy for flexible applications.

The devices exhibited excellent operational stability, attributable to PEOXA-induced enhancement in perovskite film quality and synergistic interfacial optimization. We measured operational

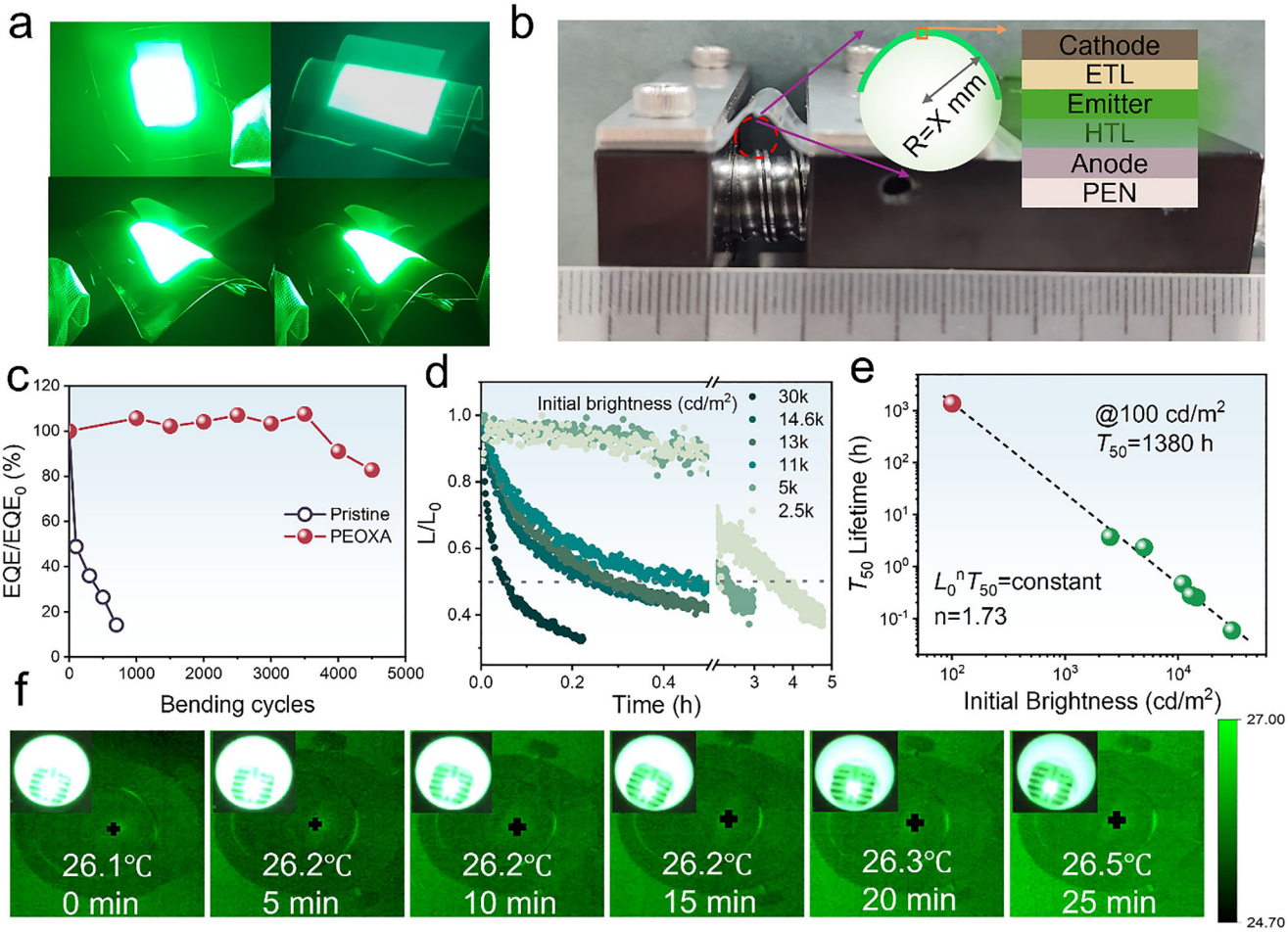

FIGURE 5 | (a) Photograph of the large-area f-PeLEDs prepared on PEN. (b) Photograph and schematic of the bending resistance test setup inside a glovebox. (c) Comparison of mechanical stability between control and PEOXA-modified devices (d) T_{50} of the champion device at various initial luminance levels. (e) Assessment of device T_{50} at a luminance of 100 cd/m^2. (f) Infrared images of the modified f-PeLEDs at different operating times. Inset shows photographs of the device taken at various operational times.

lifetimes by tracking luminance decay under constant current density. As the initial luminance increased from 2500 to 30000 cd/m^2, the corresponding T_{50} lifetime decreased from 223.2 to 3.5 min (Figure 5d). To further evaluate the device under practical operating conditions, we measured the T_{95} lifetime at an initial luminance of 1000 cd/m^2. The optimized device achieved a measured T_{95} of 3.2 h (Figure S20). Extrapolation of these data predicts a remarkable T_{50} of 1380 h at 100 cd/m^2, a value that represents a record lifetime for green f-PeLEDs (Figure 5e). We quantified Joule heating effects by monitoring device temperature during operation using infrared imaging. Measurements were performed at a constant current density of 30 mA/cm^2, producing an initial luminance of approximately 20000 cd/m^2. As predicted by our low-voltage operation principle, the device exhibited minimal temperature rise, with only 0.4°C after running 25 min (Figure 5f) [36, 37]. These results confirm that low driving voltage effectively suppresses Joule heating, thereby substantially enhancing the operational stability of flexible f-PeLEDs [54, 55]. Furthermore, the 3D polymer network formed at the interface likely suppresses ion migration along perovskite grain boundaries. To probe the ion migration dynamics, we analyzed the J-V characteristics under different scanning modes (Figure S21). The PEOXA-modified device exhibits negligible hysteresis, with a hysteresis index (HI) of 0.09, markedly lower than the 0.26 measured for the control device. Repeated cycling tests further demonstrate enhanced stability: after 20 continuous scans, the PEOXA-based device retains 87% of its initial efficiency, outperforming the control device, which degrades to 74%. These results indicate that the PEOXA-modified interface effectively enhances operational stability by passivating interfacial defects and inhibiting ion migration.

3 | Conclusions

This study proposes a polymer interfacial permeation modification strategy to synergistically enhance the efficiency, operational stability, and mechanical performance of f-PeLEDs. The introduction of functional polymer PEOXA into the HTL via a one-step spin-coating process, PEOXA can partially permeate into the perovskite emissive layer while partly remaining in the HTL, thereby forming an 3D interpenetrating network structure at the HTL/emissive layer interface and perovskite bulk regions. This unique network structure endows perovskite films with dual advantages. First, the Lewis base nature of PEOXA and its interaction with perovskite components effectively passivate

bulk and grain boundary defects in the perovskite, significantly reducing trap state density and minimizing non-radiative recombination. Second, this polymer network markedly lowers the Young's modulus of the perovskite film and enhances interlayer adhesion, thereby substantially improving the mechanical toughness and overall robustness of the film. Therefore, green f-PeLEDs fabricated via this strategy exhibit outstanding performance. The devices achieve a record-high EQE of 23.4%, a PCE of 26.7%, and a low V_T. Additionally, they demonstrate excellent mechanical bending stability, retaining 80% of their initial efficiency after 4500 bending cycles. Regarding lifetime, the estimated T_{50} lifetime of devices at 100 cd/m^2 reaches 1380 h, among the most stable f-PeLEDs. We anticipate this research offers a promising avenue for developing high-performance flexible perovskite optoelectronic devices.

Acknowledgements

This research was supported by the National Natural Science Foundation of China (52102159, 52572155 and 52272141), and the Natural Science Foundation of Fujian Province (2025J01655 and 2024J02014).

Conflicts of Interest

The authors declare no conflicts of interest.

Data Availability Statement

The data that support the findings of this study are available from the corresponding author upon reasonable request.

References

1. F. Liu, Y. Zhang, C. Ding, et al., "Highly Luminescent Phase-Stable $CsPbI_3$ Perovskite Quantum Dots Achieving Near 100% Absolute Photoluminescence Quantum Yield," *ACS Nano* 11 (2017): 10373–10383, https://doi.org/10.1021/acsnano.7b05442.

2. L. C. Schmidt, A. Pertegás, S. González-Carrero, et al., "Nontemplate Synthesis of $CH_3NH_3PbBr_3$ Perovskite Nanoparticles," *Journal of the American Chemical Society* 136 (2014): 850–853, https://doi.org/10.1021/ja4109209.

3. A. Swarnkar, R. Chulliyil, V. K. Ravi, M. Irfanullah, A. Chowdhury, and A. Nag, "Colloidal $CsPbBr_3$ Perovskite Nanocrystals: Luminescence Beyond Traditional Quantum Dots," *Angewandte Chemie International Edition* 54 (2015): 15424–15428, https://doi.org/10.1002/anie.201508276.

4. G. E. Eperon, V. M. Burlakov, P. Docampo, A. Goriely, and H. J. Snaith, "Morphological Control for High Performance, Solution-Processed Planar Heterojunction Perovskite Solar Cells," *Advanced Functional Materials* 24 (2014): 151–157, https://doi.org/10.1002/adfm.201302090.

5. T. Salim, S. Sun, Y. Abe, A. Krishna, A. C. Grimsdale, and Y. M. Lam, "Perovskite-Based Solar Cells: Impact of Morphology and Device Architecture on Device Performance," *Journal of Materials Chemistry A* 3 (2015): 8943–8969, https://doi.org/10.1039/C4TA05226A.

6. Z. Guo, Y. Liang, D. Ni, et al., "Homogeneous Phase Distribution in Q-2D Perovskites via Co-Assembly of Spacer Cations for Efficient Light-Emitting Diodes," *Advanced Materials* 35 (2023): 2302711, https://doi.org/10.1002/adma.202302711.

7. L. Zhuang, L. Zhai, Y. Li, H. Ren, M. Li, and S. P. Lau, "Mixed Dimensional 0D/3D Perovskite Heterostructure for Efficient Green Light-Emitting Diodes," *Journal of Materials Chemistry C* 9 (2021): 14318–14326, https://doi.org/10.1039/D1TC03611D.

8. T. Hu, D. Li, Q. Shan, et al., "Defect Behaviors in Perovskite Light-Emitting Diodes," *ACS Materials Letters* 3 (2021): 1702.

9. Yukta, M. K. Chini, R. Ranjan, and S. Satapathi, "Lewis Base Passivation of Quasi-2D Ruddlesden–Popper Perovskite for Order of Magnitude Photoluminescence Enhancement and Improved Stability," *ACS Applied Electronic Materials* 3 (2021): 1572–1582, https://doi.org/10.1021/acsaelm.0c01032.

10. Y. Zhao, M. Li, X. Qin, P. Yang, W.-H. Zhang, and Z. Wei, "Efficient Perovskite Light-Emitting Diodes by Buried Interface Modification With Triphenylphosphine Oxide," *ACS Applied Materials & Interfaces* 15 (2023): 3644–3650, https://doi.org/10.1021/acsami.2c19123.

11. S. Feng, Y. Shen, X. Hu, et al., "Efficient and Stable Red Perovskite Light-Emitting Diodes via Thermodynamic Crystallization Control," *Advanced Materials* 36 (2024): 2410255, https://doi.org/10.1002/adma.202410255.

12. Y. Gao, Q. Cai, Y. He, et al., "Highly Efficient Blue Light-Emitting Diodes Based on Mixed-Halide Perovskites With Reduced Chlorine Defects," *Science Advances* 10 (2024): ado5645, https://doi.org/10.1126/sciadv.ado5645.

13. Z. Xing, G. Jin, Q. Du, et al., "Ions-Induced Assembly of Perovskite Nanocomposites for Highly Efficient Light-Emitting Diodes With EQE Exceeding 30%," *Advanced Materials* 36 (2024): 2406706, https://doi.org/10.1002/adma.202406706.

14. L. Cheng, J. Huang, Y. Shen, et al., "Efficient $CsPbBr_3$ Perovskite Light-Emitting Diodes Enabled by Synergetic Morphology Control," *Advanced Optical Materials* 7 (2019): 1801534, https://doi.org/10.1002/adom.201801534.

15. J. H. Han, P. Sadhukhan, and J.-M. Myoung, "Highly Flexible and Stable Green Perovskite Light-Emitting Diodes Based on IL-Modified PEDOT:PSS Film," *Applied Surface Science* 641 (2023): 158493, https://doi.org/10.1016/j.apsusc.2023.158493.

16. W. H. Jeong, Z. Yu, L. Gregori, et al., "In Situ Cadmium Surface Passivation of Perovskite Nanocrystals for Blue LEDs," *Journal of Materials Chemistry A* 9 (2021): 26750–26757, https://doi.org/10.1039/D1TA08756H.

17. S. Y. Lee, Y. S. Nam, J. C. Yu, et al., "Highly Efficient Flexible Perovskite Light-Emitting Diodes Using the Modified PEDOT:PSS Hole Transport Layer and Polymer–Silver Nanowire Composite Electrode," *ACS Applied Materials & Interfaces* 11 (2019): 39274.

18. L. Liu, H. Yang, Z. Zhang, et al., "Photopatternable and Highly Conductive PEDOT:PSS Electrodes for Flexible Perovskite Light-Emitting Diodes," *ACS Applied Materials & Interfaces* 15 (2023): 21344.

19. H. Seo, H. Kim, J. Lee, et al., "Efficient Flexible Organic/Inorganic Hybrid Perovskite Light-Emitting Diodes Based on Graphene Anode," *Advanced Materials* 29 (2017): 1605587, https://doi.org/10.1002/adma.201605587.

20. K. Sun, Z. Bao, X. Guo, et al., "Crystallization Regulation and Defect Passivation of High-Performance Flexible Perovskite Light-Emitting Diodes Based on Novel Dielectric/Metal/Dielectric Transparent Electrodes," *Advanced Optical Materials* 12 (2024): 2301752, https://doi.org/10.1002/adom.202301752.

21. S. Sun, P. Jia, M. Lu, et al., "Enhanced Flexibility and Stability of Emissive Layer Enable High-Performance Flexible Light-Emitting Diodes by Cross-Linking of Biomass Material," *Advanced Functional Materials* 32 (2022): 2204286, https://doi.org/10.1002/adfm.202204286.

22. J. Zang, L. Cai, Y. Zou, et al., "Self-Healing Perovskite Films Enabled by Fluorinated Cross-Linked Network Targeting Flexible Light-Emitting Diode," *Advanced Optical Materials* 10 (2022): 2200566.

23. C. Liu, D. Zhang, J. Sun, et al., "Constructing Multi-Functional Polymeric-Termination Surface Enables High-Performance Flexible Perovskite LEDs," *Advanced Functional Materials* 34 (2024): 2404791, https://doi.org/10.1002/adfm.202404791.

24. M. Lu, H. Wu, X. Zhang, et al., "Highly Flexible $CsPbI_3$ Perovskite Nanocrystal Light-Emitting Diodes," *ChemNanoMat* 5 (2019): 313.

25. F. Cao, M. You, L. Kong, et al., "Mixed-Dimensional MXene-Based Composite Electrodes Enable Mechanically Stable and Efficient Flexible Perovskite Light-Emitting Diodes," *Nano Letters* 22 (2022): 4246.

26. F. Qin, M. Lu, S. Sun, et al., "Paper Substrates Based Flexible Red-Emitting Perovskite Nanocrystal Light-Emitting Diodes," *IEEE Electron Device Letters* 44 (2023): 1056–1059, https://doi.org/10.1109/LED.2023.3277852.

27. L. Zhao, N. Rolston, K. M. Lee, et al., "Influence of Bulky Organo-Ammonium Halide Additive Choice on the Flexibility and Efficiency of Perovskite Light-Emitting Devices," *Advanced Functional Materials* 28 (2018): 1802060, https://doi.org/10.1002/adfm.201802060.

28. J. Lu, X. Guan, Y. Li, et al., "Dendritic $CsSnI_3$ for Efficient and Flexible Near-Infrared Perovskite Light-Emitting Diodes," *Advanced Materials* 33 (2021): 2104414, https://doi.org/10.1002/adma.202104414.

29. Y. Shen, M.-N. Li, Y. Li, et al., "Rational Interface Engineering for Efficient Flexible Perovskite Light-Emitting Diodes," *ACS Nano* 14 (2020): 6107.

30. F. Qin, T. Li, M. Lu, et al., "Highly Efficient and Flexible Perovskite Nanocrystal Light-Emitting Diodes on Disposable Paper Substrates," *ACS Applied Materials & Interfaces* 15 (2023): 47278–47285.

31. A. Liu, I. S. Mukhin, R. M. Islamova, and J. Tian, "Flexible Perovskite Light-Emitting Diodes: Characteristics and Performance," *Advanced Functional Materials* 34 (2024): 2312209.

32. Y. Ma, J. Ge, A. K.-Y. Jen, J. You, and S. (Frank) Liu, "Polymer Boosts High Performance Perovskite Solar Cells: A Review," *Advanced Optical Materials* 12 (2024): 2301623, https://doi.org/10.1002/adom.202301623.

33. T. Li, Y. Gao, Y. Wu, et al., "Polymer Cross-Linking Strategy Enables High Performance and High Mechanical Stability Flexible Quasi-2D Perovskite Light-Emitting Diodes," *Advanced Optical Materials* 12 (2024): 2302053, https://doi.org/10.1002/adom.202302053.

34. X. Qian, Y. Shen, L.-J. Zhang, et al., "Bio-Inspired Pangolin Design for Self-Healable Flexible Perovskite Light-Emitting Diodes," *ACS Nano* 16 (2022): 17973–17981, https://doi.org/10.1021/acsnano.2c06118.

35. N. Jiang, Z. Wang, Y. Zheng, et al., "2D/3D Heterojunction Perovskite Light-Emitting Diodes With Tunable Ultrapure Blue Emissions," *Nano Energy* 97 (2022): 107181, https://doi.org/10.1016/j.nanoen.2022.107181.

36. S. Zheng, Z. Wang, N. Jiang, et al., "Ultralow Voltage–Driven Efficient and Stable Perovskite Light-Emitting Diodes," *Science Advances* 10 (2024): adp8473.

37. Y. Gao, B. Li, X. Liu, et al., "Minimizing Heat Generation in Quantum Dot Light-Emitting Diodes by Increasing Quasi-Fermi-Level Splitting," *Nature Nanotechnology* 18 (2023): 1168–1174, https://doi.org/10.1038/s41565-023-01441-z.

38. W. Cai, Y. Wang, W. Li, et al., "A Single-Step Cleaning Process for Simultaneous Removal of Surface Impurities and Passivation of Sub-Surface Defects in Perovskite Solar Cells," *Advanced Energy Materials* 14 (2024): 2304521, https://doi.org/10.1002/aenm.202304521.

39. Z. Xia, J. Jiang, A. Wang, et al., "Overall Performance Improvement of Perovskite Green LEDs by $CsPbBr_3$&Cs_4PbBr_6 Nanocrystals and Molecular Doping," *Advanced Materials* 37 (2025): 2506187, https://doi.org/10.1002/adma.202506187.

40. W. Cai, Z. Chen, Z. Li, et al., "Polymer-Assisted In Situ Growth of All-Inorganic Perovskite Nanocrystal Film for Efficient and Stable Pure-Red Light-Emitting Devices," *ACS Applied Materials & Interfaces* 10 (2018): 42564–42572, https://doi.org/10.1021/acsami.8b13418.

41. D. Kwak, S. Cho, C. Li, Y. Choi, and I. Park, "Multifunctional FA-Triflate Treatment for Efficiency and Reliability Enhancements of Quasi-2D Perovskite Light-Emitting Diodes," *Advanced Functional Materials* 35 (2025): 2422368, https://doi.org/10.1002/adfm.202422368.

42. Y. Zhao, W. Feng, M. Li, et al., "Efficient Perovskite Light-Emitting Diodes With Chemically Bonded Contact and Regulated Charge Behavior," *Nano Letters* 23 (2023): 8560–8567, https://doi.org/10.1021/acs.nanolett.3c02335.

43. W. Bai, T. Xuan, H. Zhao, et al., "Perovskite Light-Emitting Diodes With an External Quantum Efficiency Exceeding 30%," *Advanced Materials* 35 (2023): 2302283, https://doi.org/10.1002/adma.202302283.

44. Z. Luo, B. Liu, T. Zheng, et al., "High-Efficiency Sky-Blue Perovskite Light-Emitting Diodes via the Trade-Off Between the Electron–Phonon Coupling Loss and Defect Passivation," *ACS Photonics* 9 (2022): 2422–2430, https://doi.org/10.1021/acsphotonics.2c00496.

45. Y. Zhou, H. Xue, Y. Jia, G. Brocks, S. Tao, and N. Zhao, "Enhanced Incorporation of Guanidinium in Formamidinium-Based Perovskites for Efficient and Stable Photovoltaics: The Role of Cs and Br," *Advanced Functional Materials* 29 (2019): 1905739, https://doi.org/10.1002/adfm.201905739.

46. W. Li, C. Zhang, Y. Ma, et al., "In Situ Induced Core/Shell Stabilized Hybrid Perovskites via Gallium(III) Acetylacetonate Intermediate Towards Highly Efficient and Stable Solar Cells," *Energy & Environmental Science* 11 (2018): 286–293, https://doi.org/10.1039/C7EE03113K.

47. Y. Jiang, M. Cui, S. Li, et al., "Reducing the Impact of Auger Recombination in Quasi-2D Perovskite Light-Emitting Diodes," *Nature Communications* 12 (2021): 336, https://doi.org/10.1038/s41467-020-20555-9.

48. M. Amani, P. Taheri, R. Addou, et al., "Recombination Kinetics and Effects of Superacid Treatment in Sulfur- and Selenium-Based Transition Metal Dichalcogenides," *Nano Letters* 16 (2016): 2786–2791, https://doi.org/10.1021/acs.nanolett.6b00536.

49. K. Marjit, A. Das, D. Ghosh, and A. Patra, "Effect of A-Site Cations on Carrier Relaxation Dynamics of $APbBr_3$ (A = Cs/MA/FA) Perovskite Nanoplatelets," *The Journal of Physical Chemistry C* 128 (2024): 8357–8364, https://doi.org/10.1021/acs.jpcc.4c02595.

50. Z. Xiao, R. A. Kerner, N. Tran, L. Zhao, G. D. Scholes, and B. P. Rand, "Engineering Perovskite Nanocrystal Surface Termination for Light-Emitting Diodes With External Quantum Efficiency Exceeding 15%," *Advanced Functional Materials* 29 (2019): 1807284, https://doi.org/10.1002/adfm.201807284.

51. D. Zhang, Y. Fu, H. Zhan, et al., "Suppressing Thermal Quenching via Defect Passivation for Efficient Quasi-2D Perovskite Light-emitting Diodes," *Light: Science & Applications* 11 (2022): 69, https://doi.org/10.1038/s41377-022-00761-4.

52. Z. Wang, S. Zheng, N. Jiang, et al., "Minimizing Interfacial Energy Losses With Carbon Dot Bifacial Modification Layers for High-Efficiency and Stable Perovskite LEDs," *Advanced Functional Materials* 35 (2025): 2423608, https://doi.org/10.1002/adfm.202423608.

53. Z. Liu, W. Qiu, X. Peng, et al., "Perovskite Light-Emitting Diodes With EQE Exceeding 28% Through a Synergetic Dual-Additive Strategy for Defect Passivation and Nanostructure Regulation," *Advanced Materials* 33 (2021): 2103268, https://doi.org/10.1002/adma.202103268.

54. L. Kong, Y. Sun, B. Zhao, et al., "Fabrication of Red-Emitting Perovskite LEDs by Stabilizing Their Octahedral Structure," *Nature* 631 (2024): 73.

55. Q. Wu, F. Cao, W. Yu, et al., "Homogeneous ZnSeTeS Quantum Dots for Efficient and Stable Pure-Blue LEDs," *Nature* 639 (2025): 633–638, https://doi.org/10.1038/s41586-025-08645-4.

Supporting Information

Additional supporting information can be found online in the Supporting Information section.

Supporting File: lpor71194-sup-0001-SuppMat.docx.